# Tensor-Newton Reconstruction Scheme for Fluorescence Optical Tomography

**Nishgandha Patil**[1] **and Naren Naik**[1,2]

[1]Department of Electrical Engineering, Indian Institute of Technology, Kanpur, India
[2]Center for Lasers and Photonics, Indian Institute of Technology, Kanpur, India

**Abstract**— In this work, we set up the use of a Tensor-Newton scheme for solving the non-linear reconstruction problem for the fluorophore absorption coefficient, $\mu_{af}^{x}$ in $SP_N$ modeled fluorescence optical tomography. We present numerical reconstruction studies for differential uptake of fluorophore with noiseless and noisy data in test cases with varying contrast between the object and background $\mu_{af}^{x}$ value. Comparisons are presented between a first order regularising Levenberg-Marquardt scheme and two variants of the Tensor-Newton scheme. The Tensor Newton scheme is found to be more robust and performs mostly better than and at at least at par with the first order scheme in the test cases considered.

## 1. INTRODUCTION

Fluorescence optical tomography (FOT) is a structural and functional imaging modality which uses fluorescent markers to tag certain proteins to enable mapping of fluorophore properties in tissue that are indicative of physiological changes associated with pre-cancer [1]. The fluorophore is optically characterized in terms of its absorption coefficient, quantum yield and fluorescence lifetime. The inverse problem in FOT is to reconstruct the fluorophore distribution either in terms of its fluorescent yield or the flurophore absorption coefficient leading to linear and non-linear variants of the problem respectively.

Derivative based schemes are a popular choice for solving the inverse problem in tomography when set up as a residual least squares minimisation problem. To reconstruct an arbitrary optical property '$p$', a cost function $\zeta(p)$ is defined through the data residual $r(p)$ as

$$\zeta(p) = \frac{1}{2}||r(p)||^2 \tag{1}$$

In iterative schemes for minimising this cost function, at the $k^{th}$ iterate, the cost function is approximated by a model $m_k(s)$ either directly by expanding $\zeta(p^k + s)$ or indirectly by expanding $r(p^k + s)$ about the current estimate $p^k$ using the Taylor series [2, 11]. The $k^{th}$ update $s^k$ is then computed as the model minimiser

$$s^k = \arg\min_s m_k(s) \tag{2}$$

Schemes based on first order (FO) expansion of the residual are commonly used to solve the residual minimisation problem. For a detailed discussion on various FO reconstruction schemes for the linear and non-linear problems in FOT, the reader is referred to [3, 4] and references therein. Few works in literature discuss the use of quadratic or higher order expansion based schemes for solving the tomographic inverse problem. In [5], Hettlich and Rundell have developed a second order scheme to solve the inverse problem as a non-linear system of equations, referred to as the second degree scheme, using a predictor-corrector approach which shows faster convergence in test cases considered by them. This scheme is used to solve the diffuse optical tomography problem in a non-linear conjugate gradient framework by Kanmani and Vasu in [6] and seen to provide better contrast recovery. In [7], Roy and Muraca demonstrate a truncated Newton scheme for solving the non-linear FOT problem using the diffusion approximation.

These studies indicate that the use of second order (SO) expansion based schemes in general affords better contrast recovery, noise tolerance and in some cases a faster convergence than their FO counterparts.

However the use of SO reconstruction schemes for FOT has remain largely unexplored. The main impediment to the use of SO schemes is the computational effort required to evaluate the second order derivatives. The development of a computationally efficient adjoint based scheme for evaluating the second order derivative (Hessian) for $SP_N$ modeled FOT by us in [8] makes it feasible to investigate the use of SO schemes to solve the FOT inverse problem. In the same work [8], we also demonstrate the use of the second degree scheme of Hettlich and Rundell [5] in a regularising Levenberg-Marquardt framework to solve the non-linear inverse problem in FOT.

In the optimisation related literature, higher order schemes for solving the least squares problem have been discussed in [2, 9–11]. In [2] and [9] the higher order terms are approximated using function and derivative values, while in [10] and [11] the exact higher order derivatives are used. For the nonlinear least squares minimisation problem, Transtrum and Sethna [10] have proposed a second order correction to the FO update evaluated using the Levenberg-Marquardt scheme which resulted in improvements in fit quality and success rate in numerical studies on test problems. In a recent work, Gould et al. [11] describe a Tensor-Newton scheme that uses second order derivatives, which results in a quartic model to the cost function and is more robust than other schemes for solving non-linear least squares problems considered in the study.

In the Tensor-Newton scheme the $i^{th}$ component of the residual $r_i(p+s)$ is approximated about the current estimate of '$p$' by its second order Taylor series approximation $t_i(p,s)$. (The '$p$' dependence of $t_i(p,s)$ is suppressed in the rest of the text for notational simplicity.) The cost function $\zeta(p)$ is then modeled as the resulting quartic function in '$s$' and the $k^{th}$ update step $s^k$ is evaluated by solving the non-linear sub-problem in Eq. (2) using any least squares minimisation scheme. The Tensor-Newton scheme minimises the number of function and derivative evaluations with respect to '$p$' since evaluating and updating the gradient of $t_i(s)$ while minimising $m_k(s)$, does not require re-evaluating the Jacobian and Hessian with respect to '$p$'.

In the present work, we set up the use of a Tensor-Newton scheme for solving the nonlinear reconstruction problem for the fluorophore absorption coefficient at excitation wavelength $\mu_{af}^x$. We use the $SP_N$ approximation, which is known to be more accurate than the diffusion approximation [12], to model light transport through the medium. The exact Jacobian and Hessian required are evaluated using adjoint-based schemes detailed by us in [4] and [8] respectively. We present numerical reconstruction studies considering differential uptake of fluorophore for noiseless and noisy data in test cases with varying contrast between the object(s) and the background.

In Section 2 we describe the forward problem of modeling fluorescent light transport using the $SP_3$ approximation. The non-linear inverse problem is described in Section 3, and the Tensor-Newton reconstruction algorithm with its two variants is detailed in Section 4. Numerical studies are presented in Section 5 and the conclusions in Section 6.

## 2. THE FORWARD PROBLEM

Consider a closed domain $V$, optically characterized by its intrinsic absorption coefficient, $\mu_{ai}^{x/m}[\mathrm{cm}^{-1}]$, scattering coefficient $\mu_s^{x/m}[\mathrm{cm}^{-1}]$, anisotropy factor $g[-]$ and refractive index $n_{med}[-]$, with '$x/m$' denoting quantities at excitation and emission wavelength respectively. The intrinsic/extrinsic fluorophore distributed in the medium is characterized by the fluorophore absorption coefficient $\mu_{af}^{x/m}\,[\mathrm{cm}^{-1}]$, quantum yield $\eta[-]$ and fluorescence lifetime $\tau\,[\mathrm{ns}]$. The domain is illuminated with an isotropic source $S(r)$ located on the boundary and modulated at a frequency of $f\,[\mathrm{MHz}]$. The coupled set of equations modeling the generation and propagation of fluorescent radiation through this domain, using the $SP_3$ approximation, is given by [4, 12]:

$$-\nabla \cdot C^{\nabla x} \nabla \varphi^x + C^x \varphi^x = 0 \tag{3a}$$

$$-\nabla \cdot C^{\nabla m} \nabla \varphi^m + C^m \varphi^m = C^\beta \varphi^x \tag{3b}$$

with partially reflecting boundary conditions,

$$C^{\nabla bx}(n.\nabla\varphi^x) + C^{bx}\varphi^x = C^{Sx} \tag{3c}$$

$$C^{\nabla bm}(n.\nabla\varphi^m) + C^{bm}\varphi^m = 0 \tag{3d}$$

where

$$C^{\nabla x/m} = \begin{pmatrix} \frac{1}{3\mu_{a1}^{x/m}} I & 0 \\ 0 & \frac{1}{7\mu_{a3}^{x/m}} I \end{pmatrix} \quad C^{\beta} = \begin{pmatrix} \beta & -\frac{2}{3}\beta \\ -\frac{2}{3}\beta & \frac{4}{9}\beta \end{pmatrix} \quad C^{x/m} = \begin{pmatrix} \mu_{a0}^{x/m} & -\frac{2}{3}\mu_{a0}^{x/m} \\ -\frac{2}{3}\mu_{a0}^{x/m} & (\frac{4}{9}\mu_{a0}^{x/m} + \frac{5}{9}\mu_{a2}^{x/m}) \end{pmatrix}$$

$$C^{bx/m} = \begin{pmatrix} (\frac{1}{2} + A_1) & -(\frac{1}{8} + C_1) \\ -(\frac{1}{8} + C_2) & (\frac{7}{24} + A_2) \end{pmatrix} \quad C^{\nabla bx/m} = \begin{pmatrix} \frac{1+B_1}{3\mu_{a1}^{x/m}} & -\frac{D_1}{\mu_{a3}^{x/m}} \\ -\frac{D_2}{\mu_{a1}^{x/m}} & \frac{1+B_2}{7\mu_{a3}^{x/m}} \end{pmatrix} \quad \varphi^{x/m} = \begin{pmatrix} \varphi_1^{x/m} \\ \varphi_2^{x/m} \end{pmatrix}$$

$$C^{Sx} = \begin{pmatrix} \int_{\Omega\cdot n<0} S(r) 2|\Omega\cdot n| d\Omega \\ \int_{\Omega\cdot n<0} S(r)(5|\Omega\cdot n|^3 - 3|\Omega\cdot n|) d\Omega \end{pmatrix} \quad \underline{\nabla} = \begin{pmatrix} \frac{\partial}{\partial x} \\ \frac{\partial}{\partial y} \end{pmatrix}, \quad \nabla = \begin{pmatrix} \underline{\nabla} & 0 \\ 0 & \underline{\nabla} \end{pmatrix}, \quad I = \begin{pmatrix} 1 & 0 \\ 0 & 1 \end{pmatrix}$$

$$n = \begin{pmatrix} n_x \\ n_y \end{pmatrix}, \quad n\cdot\nabla\varphi^{(x/m)} = \begin{pmatrix} n\cdot\nabla\varphi_1^{x/m} \\ n\cdot\nabla\varphi_2^{x/m} \end{pmatrix} \qquad \beta = \frac{\eta\mu_{af}^{x}}{1 - j\omega\tau}, \quad \omega = 2\pi f$$

Here '$\Omega$' is the direction vector and '$n$' is the normal to the boundary $\partial V$. $\varphi_{1,2}^{x/m}$ are the composite moments of fluence as defined in [12] and the absorption moments are defined as

$$\mu_{al}^{x/m} = \mu_{ai}^{x/m} + \mu_{af}^{x/m} + \left(1 - g^l\right)\mu_s^{x/m} + \frac{j\omega}{c}, \quad l = 0, 1, 2 \tag{4}$$

The measurement considered is the exiting partial current $j^+$, evaluated at detector locations $r_j \in \partial V$. For the FOT problem we only consider measurements at the emission wavelength, given by

$$j^{+m}(r_j) = C^{Jm}\varphi^m - C^{\nabla Jm} n\cdot\nabla\varphi^m \tag{5}$$

where

$$C^{Jm} = \left( \left(\frac{1}{4} + J_0\right) \quad \left[\left(-\frac{2}{3}\right)\left(\frac{1}{4} + J_0\right) + \frac{1}{3}\left(\frac{5}{16} + J_2\right)\right] \right)\delta(r - r_j), \ C^{\nabla Jm} = \left( \frac{(0.5+J_1)}{3\mu_{a1}^m} \quad \frac{J_3}{7\mu_{a3}^m} \right)\delta(r - r_j).$$

The coefficients $A_n, B_n, C_n, D_n$ and $J_n$ are evaluated in [12].

## 3. THE INVERSE PROBLEM

In the non-linear least squares minimisation approach to solve the FOT inverse problem of reconstructing the optical property $p = \mu_{af}^x$, the cost function $\zeta(p)$ is defined as

$$\zeta(p) \triangleq \frac{1}{2}||r(p)||^2 = \frac{1}{2}||\mathcal{F}(p) - j_{meas}^+||^2 \tag{6}$$

where $\mathcal{F}(\cdot)$ is an operator that denotes the tomographic process and $j_{meas}^+$ denotes experimental measurements. Beginning at an initial estimate $p^0$, the $k^{th}$ update $s^k$ is evaluated as

$$s^k = \arg\min_s m(s) \tag{7}$$

where $m(s)$ is a model for $\zeta(p + s)$.

In Gauss-Newton type schemes, $m_{GN}(s)$ is defined through a first order Taylor series expansion of the residual $r(p + s)$ as [2, 11]

$$m_{GN}(s) \triangleq \frac{1}{2}||r(p) + J(p)s||^2 \tag{8}$$

where the Jacobian $J(p) \triangleq \nabla_p r = \mathcal{F}'$. In the regularising Levenberg-Marquadt [4, 13] implementation of this scheme, the $k^{th}$ update $s^k$, is evaluated by solving

$$\left(\left(J^k\right)^T J^k + \lambda^k L^T L\right) s^k = -\left(J^k\right)^T r^k \tag{9}$$

where $\lambda^k$ is the Levenberg-Marquardt parameter and the matrix '$L$' is the graph Laplacian corresponding to the spatial basis used for reconstruction [14]. Since this scheme uses only the first order (FO) derivatives, in the rest of the text, we refer to this scheme as the first order (FO) scheme.

The Tensor Newton scheme makes use of a second order expansion of the residual $r(p+s)$, to define the model $m_{TN}(s)$ as

$$m_{TN}(s) \triangleq \frac{1}{2}||t(s)||^2 = \frac{1}{2}\sum_{i=1}^{N} t_i^2 \tag{10}$$

$$t_i(s) \triangleq r_i(p+s) = r_i(p) + J_i(p)s + \frac{1}{2}s^T H_i(p)s \tag{11}$$

with $r_i$, $J_i$ and $H_i \triangleq \nabla_{pp} r_i = \mathcal{F}''$ being the residual, Jacobian and Hessian respectively corresponding to the $i^{th}$ measurement. The vector $t(s)$ and the tensor $H(p)$ are formed by stacking $t_i$ and $H_i$ respectively. We denote by $((s^T \cdot H(p))s)$ the vector formed such that $((s^T \cdot H(p))s)_i = s^T H_i(p)s$. It is easy to see that the subproblem in Eq. (2) (with $m_{TN}(s)$ as given above in Eq. 10) is itself a non-linear least squares problem and can be solved by using any least squares minimisation routine. In the present work, we use a first order scheme to solve this sub-problem. Thus in each iteration of the Tensor Newton scheme, the parameter $p$ is updated as $p^{k+1} = p^k + s^k$, where $s^k$ is obtained by solving the subproblem in Eq. (2) using a first order iterative scheme. Denoting the gradient of $t(s)$ as,

$$\nabla_s t = J(p) + (s^T \cdot H(p)) \tag{12}$$

the $m^{th}$ update to $s$, denoted as $q^m$, is evaluated by solving

$$\left((\nabla_s t^m)^T(\nabla_s t^m) + \lambda^m L^T L\right) q^m = -(\nabla_s t^m)^T t^m \tag{13}$$

and $\tilde{s}$, the current estimate of $s^k$, is updated as $\tilde{s}^{m+1} = \tilde{s}^m + q^m$. In the next section, we present the algorithm for the implementation of the Tensor Newton scheme.

## 4. THE TENSOR-NEWTON RECONSTRUCTION ALGORITHM

Algorithm 1 describes the basic Tensor-Newton scheme in the regularising Levenberg-Marquardt framework. The Levenberg-Marquardt parameter $\lambda$ can be updated using any of the strategies described in [15]. In our work, $\lambda$ is decreased by a factor of 3 for very successful updates, increased by a factor of 2 for very poor updates and left unchanged otherwise.

**Algorithm 1** The tensor newton reconstruction algorithm.

**Data:** Given $p^0, \lambda^0, j^+_{meas}, L$
Evaluate $r(p^0)$, $\zeta(p^0)$;
k=0;
**while** *termination criteria are not met* **do**
  Evaluate $r(p^k)$, $J^k = \mathcal{F}'(p^k)$ and $H^k = \mathcal{F}''(p^k)$;
  Obtain $s^k$ by solving the subproblem in eq. 2 using either Algorithm 2 or Algorithm 3;
  Evaluate $\zeta(p^k + s^k)$ and compute goodness of fit $\rho = \frac{\zeta(p^k+s^k)-\zeta(p^k)}{m_{TN}(s^k)-m_{TN}(0)}$;
  **if** $\rho > \rho_{accept}$ **then**
    $p^{k+1} = p^k + s^k$;
    $k = k+1$;
  **end**
  Update $\lambda^k$;
**end**
**Result:** Return $p^k$

We solve the subproblem in Eq. (2) using two different schemes described in Algorithms 2 and 3. In the first scheme, referred to as TN1 (Algorithm 2), in each iterate, $t(s+q)$ is expanded about the current estimate $\tilde{s}^m$, using a first order Taylor series and a sequence of updates $\{q^m\}$ is generated, by solving the system of equations so obtained. The current value of the estimate $\tilde{s}^m$ of $s^k$, is updated as $\tilde{s}^{m+1} = \tilde{s}^m + q^m$.

**Algorithm 2** The TN1 scheme for solving the Tensor-Newton sub-problem.

**Data:** Given $p^k, r(p^k), J^k, H^k, \lambda^k, L$
$m = 0$;
**while** *termination criteria are not met* **do**
  Set $\tilde{s}^0 = 0, \lambda_{in}^m = \lambda^k, t^0 = r(p^k)$;
  **for** *m=0,1,..* **do**
    Evaluate $m_{TN}(\tilde{s}^m)$;
    Set $\nabla_s t = J(p^k) + \tilde{s}^m \cdot H(p^k)$;
    Obtain $q^m$ by solving: $\left((\nabla_s t)^T(\nabla_s t) + \lambda_{in}^m L^T L\right) q^m = -(\nabla_s t)^T t^m$;
    **if** $m_{TN}(\tilde{s}^m + q^m) < m_{TN}(\tilde{s}^m)$ **then**
      $\tilde{s}^{m+1} = \tilde{s}^m + q^m$;
      $t^{m+1} = r(p^k + \tilde{s}^{m+1})$;
      $m = m + 1$;
    **end**
    **if** *Termination criteria are met* **then**
      break;
    **end**
    Update $\lambda_{in}^m$
  **end**
**end**
**Result:** Return the $k^{th}$ update to $s^k = \tilde{s}^m$

In the second scheme, referred to as TN2 (Algorithm 3), we make use of a predictor-corrector approach to obtain $s^k$. Beginning with a prediction of $s^k$, denoted as $\tilde{s} = 0$, we obtain its corrected estimate $\tilde{s} = \alpha q^m$ by solving

$$\left((\nabla_s t)^T(\nabla_s t) + \lambda_{in}^m L^T L\right) q^m = -(\nabla_s t)^T t^0 \tag{14}$$

a maximum of $M$ times. Here $\alpha$ is determined using a line search routine. This makes it similar to the second order scheme described in [5] and used by us in its frozen Hessian variant in [8], with the corrector step iterated a maximum of M times. However instead of heuristically fixing the number iterations of the corrector step, by using a model minimisation criteria for $m_{TN}(s)$, the present scheme allows to adaptively vary the number of iterations over the corrector.

**Algorithm 3** The TN2 scheme for solving the Tensor-Newton sub-problem.

**Data:** Given $p^k, r(p^k), J^k, H^k, \lambda^k, L$
$m = 0$;
**while** *termination criteria are not met* **do**
  Set $\tilde{s} = 0, \lambda_{in}^m = \lambda^k, t^0 = r(p^k)$;
  **for** *m=0,1,..* **do**
    Evaluate $m_{TN}(\tilde{s})$;
    Set $\nabla_s t = J(p^k) + \tilde{s} \cdot H(p^k)$;
    Obtain $q^m$ by solving: $\left((\nabla_s t)^T(\nabla_s t) + \lambda_{in}^m L^T L\right) q^m = -(\nabla_s t)^T t^0$;
    **if** $m_{TN}(\alpha q^m) < m_{TN}(\tilde{s})$ **then**
      $\tilde{s} = \alpha q^m$;
      $m = m + 1$;
    **end**
    **if** *Termination criteria are met* **then**
      break;
    **end**
  **end**
**end**
**Result:** Return the $k^{th}$ update to $s^k = \tilde{s}$

When starting with an initial estimate, $\tilde{s} = 0$ in each iterate, both the schemes for solving the sub-problem exhibit a built in flexibility of choosing the first order step if it is found to be optimal over the second order step.

## 5. NUMERICAL STUDIES

The computational domain is taken to be a square of size $2 \times 2$ cm. Ten detectors are located along each edge of the square and the excitation source of strength 1 mW, modulated at 100 MHz is placed sequentially at the center of each edge. Measurements are taken on all sides, and a total of 160 complex measurements are used in each dataset. The data is logarithmically scaled prior to its use in the reconstruction algorithm. The optical properties of the medium and the fluorophore are taken as that of Phantom 1 in [4] and are listed in Table 1.

Table 1. Optical properties of the medium and fluorophore. The subscripts $i/f$ denote quantities related to the background/fluorophore and the superscripts $x/m$ indicate quantities at excitation/emission wavelength respectively. Quantities without superscripts are taken to be indepndent of wavelength in this study.

| | $\mu_{ai}^x$ | $\mu_{af}^x$ | $\mu_{ai}^m$ | $\mu_{af}^m$ | $\mu_s^x$ | $\mu_s^m$ | $g$ | $n_{med}$ | $\eta_f$ | $\tau_f$ (ns) |
|---|---|---|---|---|---|---|---|---|---|---|
| Phantom | 0.031 | 0.006 | $0.7987\mu_{ai}^x$ | $0.0846\mu_{af}^x$ | 54.75 | $0.732\mu_s^x$ | 0.8 | 1.37 | 0.016 | 0.56 |

The Galerkin's finite element method [16] is used to solve the forward problem on a structured mesh with mesh spacing of 0.05 cm (3200 elements). The simulated data is generated on a finer mesh with spacing of 0.025 cm (12800 elements).

We present reconstruction studies for four test phantoms, each with 2 circular inhomogeneities centered at $(-0.5, 0)$ and $(0.5, 0)$ having varying values of $\mu_{af}^x$, for both noiseless and noisy datasets described in Table 2 using (a) the first order regularising Levenberg Marquardt scheme [4] (FO) (b) the Tensor Newton scheme using Algorithm 2 (TN1) and (c) the Tensor Newton scheme using Algorithm 3 (TN2). The different datasets differ in terms of the contrast ratio between the $\mu_{af}^x$ values of the object and the background. We consider test cases with low contrast (LC-N0, LC-N1), moderate contrast (MC-N0, MC-N1) and high contrast (HC-N0, HC-N1) for objects of same size with varying $\mu_{af}^x$ values. We also present reconstructions for a test case (LS-N0, LS-N1) with two objects of unequal radii having the same $\mu_{af}^x$ value. In each case the reconstructions are initialised with a homogeneous value of 0.006 cm$^{-1}$. The reconstructed parameter values are thresholded at $0.2\max(\mu_{af}^{x,rec})$ prior to plotting and analysis.

Table 2. Description of datasets used in the study.

| Dataset | center of inhomogeneity | | radius (in cm) of | | $\mu_{af}^{x,act}$ cm$^{-1}$ | | SNR | |
|---|---|---|---|---|---|---|---|---|
| | Object 1 | Object 2 | Object 1 | Object 2 | Object 1 | Object 2 | N0 | N1 |
| LC | $(-0.5, 0)$ | (0.5,0) | 0.20 | 0.20 | 0.03 | 0.09 | inf | 25 |
| MC | $(-0.5, 0)$ | (0.5,0) | 0.20 | 0.20 | 0.24 | 0.30 | inf | 30 |
| HC | $(-0.5, 0)$ | (0.5,0) | 0.20 | 0.20 | 0.48 | 0.12 | inf | 25 |
| LS | $(-0.5, 0)$ | (0.5,0) | 0.32 | 0.20 | 0.30 | 0.30 | inf | 25 |

We compare the reconstructions obtained using the three schemes with respect to (a) the correlation coefficient and the (b) deviation factor defined as [17]

$$\rho_c = \frac{\sum_{i=1}^{N_e}(\mu_{af,i}^{x,rec} - \bar{\mu}_{af}^{x,rec})(\mu_{af,i}^{x,act} - \bar{\mu}_{af}^{x,act})}{(N_e - 1)\Delta\mu_{af}^{x,rec}\Delta\mu_{af}^{x,act}} \qquad \rho_d = \frac{\sqrt{(1/N_e)\sum_{i=1}^{N_e}(\mu_{af,i}^{x,rec} - \mu_{af,i}^{x,act})^2}}{\Delta\mu_{af}^{x,act}} \tag{15}$$

Here '$N_e$' is the total number of elements, $\bar{\mu}_{af}^{x,rec}, \bar{\mu}_{af}^{x,act}$ are the mean values and $\Delta\mu_{af}^{x,rec}, \Delta\mu_{af}^{x,act}$ are the standard deviations of the reconstructed and original spatial parameter distributions. The error measures evaluated over a region of interest, defined in this study as a rectangle of $2 \times 1$ cm centered at the origin, are listed in Table 3. A good match between the actual and reconstructed values is indicated by a higher correlation coefficient and a lower deviation factor.

### 5.1. Low Contrast Test Case

Reconstructions for the low contrast data sets LC-N0 and LC-N1 are plotted in Figure 1. For both datasets, the reconstructed values and the error metrics (ref. Table 3) obtained are similar using all the three schemes, and the parameter value is substantially underestimated. The TN1

Table 3. Error measures for the First order (FO) and Tensor Newton reconstruction schemes using Algorithm 2 (TN1) and Algorithm 3 (TN2) with noiseless (N0) and noisy data (N1).

| | $\rho_c$ | | | $\rho_d$ | | | $\max \mu_{af}^{x,rec}$ cm$^{-1}$ (Object 1, Object 2) | | |
|---|---|---|---|---|---|---|---|---|---|
| Dataset | FO | TN1 | TN2 | FO | TN1 | TN2 | FO | TN1 | TN2 |
| LC-N0 | 0.69 | 0.81 | 0.66 | 0.76 | 0.65 | 0.78 | (.0145,.0381) | (.0183,.0485) | (.0134,.0369) |
| LC-N1 | 0.68 | 0.65 | 0.72 | 0.76 | 0.78 | 0.72 | (.0150,.0404) | (.0213,.0466) | (.0149,.0447) |
| MC-N0 | 0.79 | 0.94 | 0.88 | 0.67 | 0.36 | 0.53 | (.1203,.1494) | (.2294,.2904) | (.1631,.2052) |
| MC-N1 | 0.68 | 0.79 | 0.81 | 0.79 | 0.66 | 0.64 | (.0739,.1153) | (.1011,.1846) | (.1089,.1798) |
| HC-N0 | 0.77 | 0.83 | 0.88 | 0.69 | 0.62 | 0.52 | (.2102,.0584) | (.2574,.0706) | (.3320,.0839) |
| HC-N1 | 0.81 | 0.86 | 0.91 | 0.65 | 0.46 | 0.57 | (.2355,.0711) | (.2882,.0781) | (.4011,.1011) |
| LS-N0 | 0.90 | 0.91 | 0.89 | 0.43 | 0.42 | 0.47 | (.3927,.1722) | (.5259,.1453) | (0.3798,.1453) |
| LS-N1 | 0.80 | 0.81 | 0.81 | 0.61 | 0.58 | 0.62 | (.4399,.1485) | (.4145,.1325) | (0.5323,.1652) |

scheme shows a clear split between the two objects for LC-N0 which is not seen with the other schemes. With noisy data (LC-N1), the TN1 and TN2 schemes can clearly distinguish between the two objects while the FO scheme cannot; however many artifacts are observed in the TN1 reconstruction.

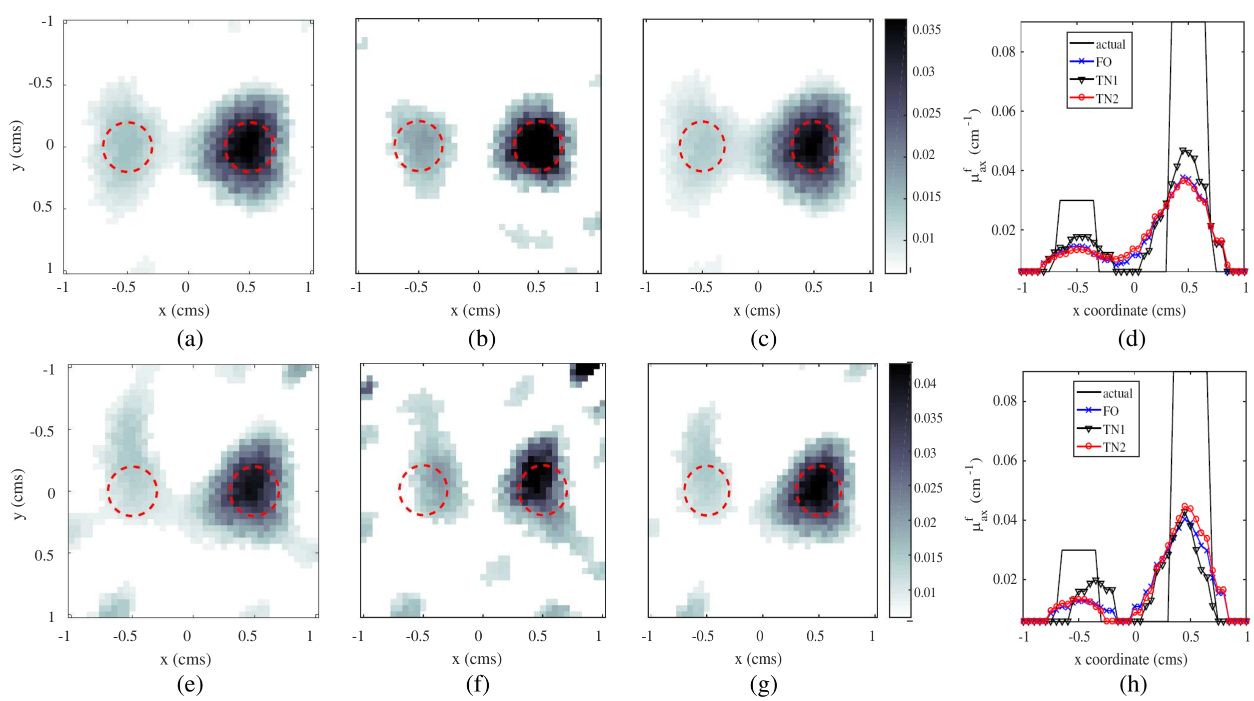


Figure 1. Reconstructions for datasets LC-N0 (top row) and LC-N1 (bottom row) using the first order (FO) scheme (left column), the Tensor Newton scheme with Algorithm 3 (TN1, central column) and with Algorithm 3 (TN2, right column). The dashed red circles indicate the actual inhomogeneities. Plots (d) and (h) show the cross sectional values of $\mu_{af}^x$ along $y = 0$ for noise levels N0 and N1 respectively.

### 5.2. Moderate Contrast Test Case

It can be seen from Figure 2 and Table 3 that, the TN1 and TN2 reconstruction schemes demonstrate better localisation and provide more accurate parameter estimates as compared to the FO scheme for both datasets. While the TN1 scheme performs distinctly better than the other two schemes for the noiseless case, it's performance is comparable to the TN2 scheme for the noisy case.

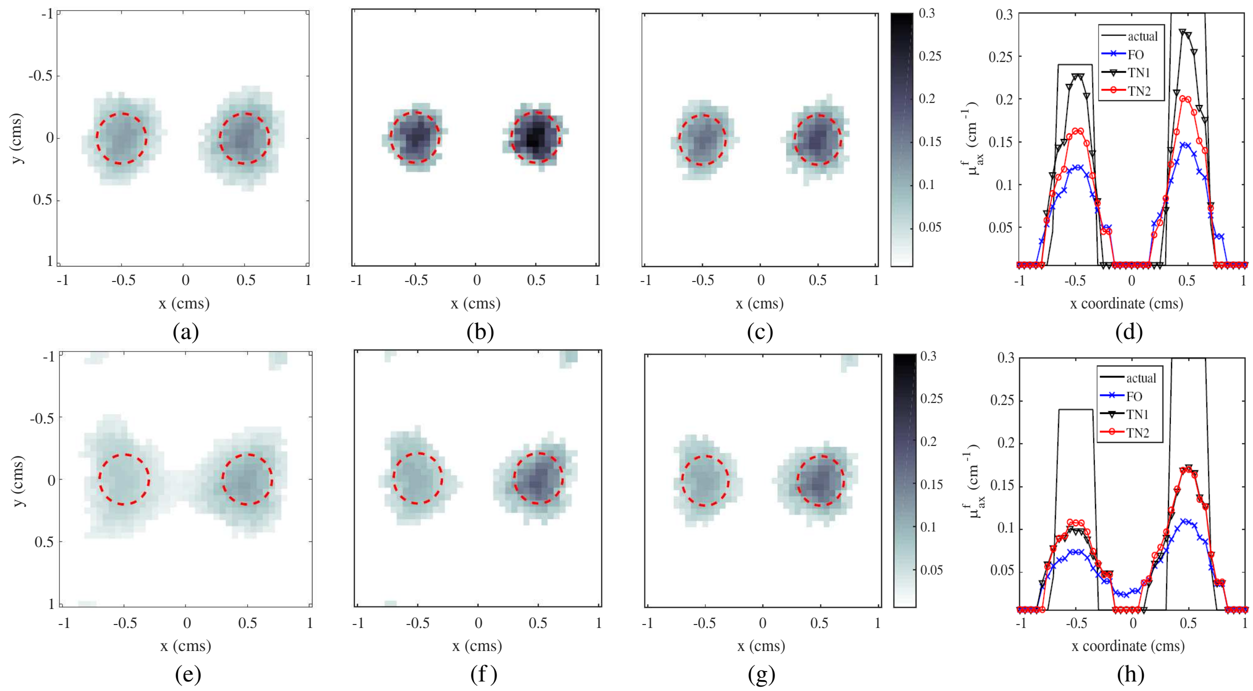


Figure 2. Reconstructions for datasets MC-N0 (top row) and MC-N1 (bottom row) using the first order (FO) scheme (left column), the Tensor Newton scheme with Algorithm 3 (TN1, central column) and with Algorithm 3 (TN2, right column). The dashed red circles indicate the actual inhomogeneities.Plots (d) and (h) show the cross sectional values of $\mu_{af}^{x}$ along $y = 0$ for noise levels N0 and N1 respectively.

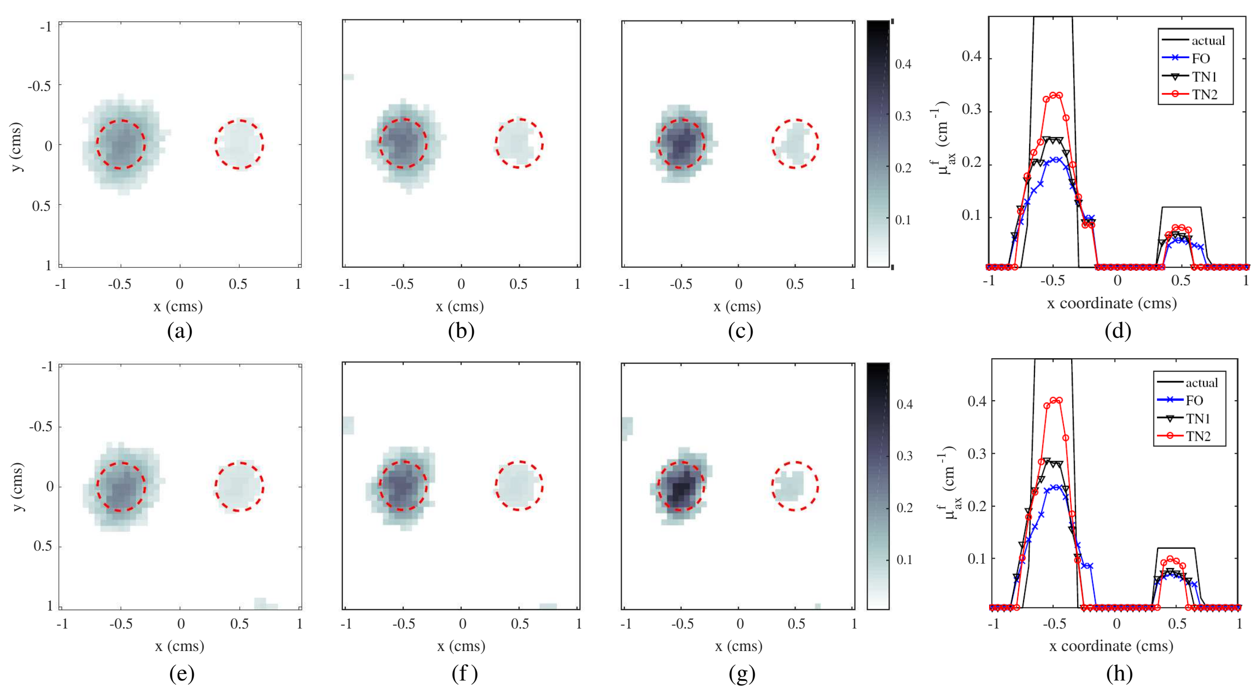


Figure 3. Reconstructions for datasets HC-N0 (top row) and HC-N1 (bottom row) using the first order (FO) scheme (left column), the Tensor Newton scheme with Algorithm 3 (TN1, central column) and with Algorithm 3 (TN2, right column). The dashed red circles indicate the actual inhomogeneities. Plots (d) and (h) show the cross sectional values of $\mu_{af}^{x}$ along $y = 0$ for noise levels N0 and N1 respectively.

### 5.3. High Contrast Test Case

Consistent with the observations in the previous case, one can note from Figure 3 that better parameter estimates and localisation is obtained with the TN1 and TN2 schemes. While the TN1 scheme performs marginally better, the TN2 scheme distinctly outperforms the other two schemes in terms of the recovered parameter value.

### 5.4. Test Case with Inhomogeneities of Different Size

In this case (Figure 4), all three schemes perform at par in that they overestimate the parameter value in the larger inhomogeneity and underestimate it in the smaller inhomogeneity.

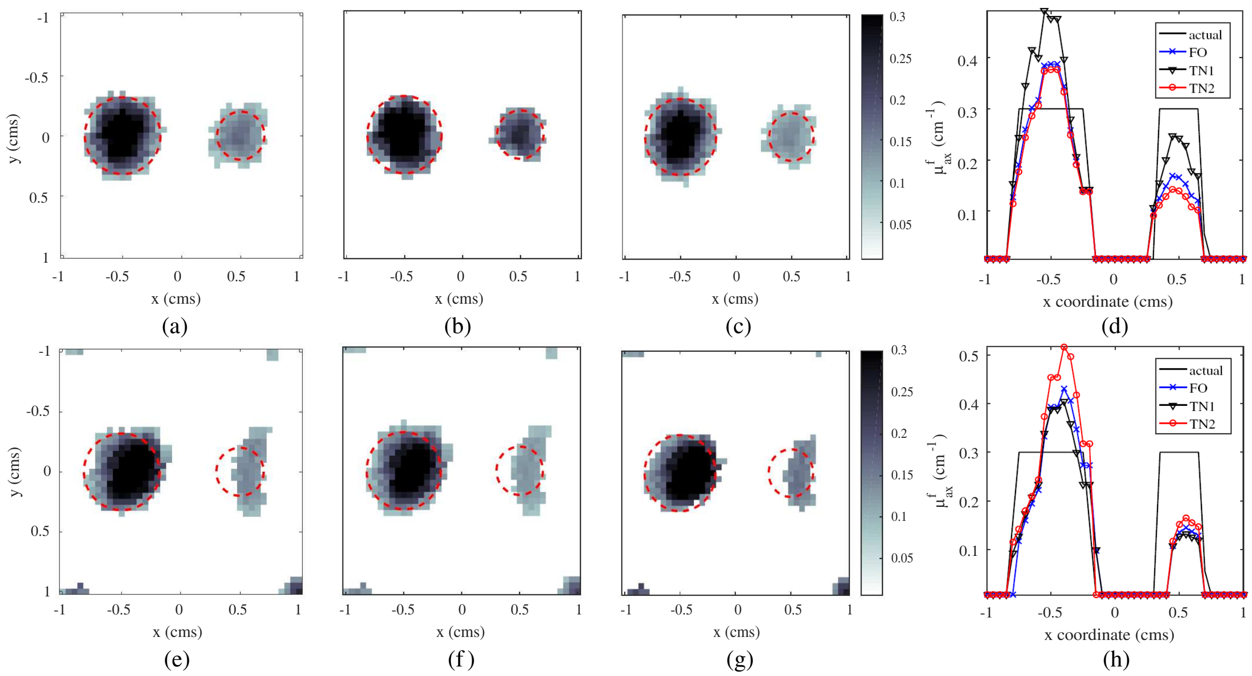


Figure 4. Reconstructions for datasets LS-N0 (top row) and LS-N1 (bottom row) using the first order (FO) scheme (left column), the Tensor Newton scheme with Algorithm 3 (TN1, central column) and with Algorithm 3 (TN2, right column). The dashed red circles indicate the actual inhomogeneities.Plots (d) and (h) show the cross sectional values of $\mu_{af}^{x}$ along $y = 0$ for noise levels N0 and N1 respectively.

## 6. CONCLUSION

In this manuscript we have presented two variants of a Tensor Newton reconstruction scheme for $SP_N$ approximation based FOT. The scheme allows for an efficient reuse of the Jacobian and Hessian evaluated at each iterate. Another feature of this scheme is the built-in flexibility to use the first order step if it is found to be optimal with respect to the model $m_{TN}(s)$. Numerical reconstruction studies are presented for phantoms with varying contrast ratios between the object and the background as well for objects of different sizes.

Our study shows that the both the variants of the Tensor Newton scheme exhibit performance which is at least at par with if not better than the first order scheme. For test cases with moderate to high contrast between the object and the background, the Tensor Newton scheme provides better parameter estimates. These observations are consistent with other works in literature that use second-order derivative based reconstruction schemes. Between the two variants of the scheme, the TN2 scheme using algorithm 3 is more robust in presence of noise.

However due to the need to evaluate the second order derivatives in each iterate, the Tensor Newton scheme is computationally expensive. More efficient approaches can possibly be developed by exploiting the built-in hybrid nature of the scheme or by implementing variants of the scheme with frozen second derivatives.

### REFERENCES

1. Vasilis, N., "Fluorescence molecular imaging," *Annu. Rev. Biomed. Eng.*, Vol. 8, No. 1, 1–33, 2006.

2. Dennis, J. and R Schnabel, "Numerical methods for unconstrained optimization and nonlinear equations," *SIAM*, Vol. 16, 2006.
3. Darne, C., Y. Lu, and E. Sevick-Muraca, "Small animal fluorescence and bioluminscence tomography: a review of approaches, algorithms and technology update," *Phys. Med. Biol.*, Vol. 59, R1–R84, 2014.
4. Naik, N., N. Patil, Y. Yadav, J. Eriksson, and A. Pradhan, "Fully nonlinear $SP_3$ approximation based fluorescence optical tomography," *IEEE Trans. Med. Imaging*, Vol. 36, 2308–2318, 2017.
5. Hettlich, F. and W. Rundell, "A second degree method for nonlinear inverse problems," *SIAM J. Numer. Anal.,*, Vol. 37, No. 2, 587–620, 1999.
6. Kanmani, B. and R. Vasu, "Diffuse optical tomography through solving a system of quadratic equations: theory and simulations," *Phys. Med. Biol.*, Vol. 51, No. 4, 2006.
7. Roy, R. and E. Sevick-Muraca, "Truncated Newtons optimization scheme for absorption and fluorescence optical tomography: Part I theory and formulation," *Opt. Express*, Vol. 4, No. 10, 353–371, 1999.
8. Patil, N. and N. Naik, "Second-order adjoint sensitivities for fluorescence optical tomography based on the spn approximation," 2019 (submitted).
9. Bouaricha, A. and R. Schnabel, "Tensor methods for large, sparse systems of nonlinear equations," Preprint MCS-P473-1094, Mathematics and Computer Science Division, Argonne National Laboratory, 1994.
10. Transtrum, M. and J. Sethna, "Improvements to the Levenberg-Marquardt algorithm for nonlinear least squares minimisation," arXiv preprint arXiv:1201.5885, 2012.
11. Gould, N. I. M., T. Rees, and J. A. Scott, "A higher order method for solving nonlinear least-squares problems," RAL Preprint RAL-P-2017-010, STFC Rutherford Appleton Laboratory, 2017.
12. Klose, A. and E. Larsen, "Light transport in biological tissue based on the simplified spherical harmonics equations," *J. Comput. Phys.*, Vol. 220, No. 1, 2006.
13. Hanke, M., "A regularizing Levenberg-Marquardt scheme, with applications to inverse groundwater filtration problems," *Inverse Probl.*, Vol. 13, No. 1, 1997.
14. Schweiger, M., S. Arridge, and N. Ilkka, "Gauss-Newton method for image reconstruction in diffuse optical tomography," *Phys. Med. Biol.*, Vol. 50, No. 10, 2005.
15. Conn, A., N. Gould, and P. Toint, "Trust region methods," *SIAM*, 2000.
16. Jin, J., *The Finite Element Method in Electromagnetics*, John Wiley & Sons, 2014.
17. Klose, A. and A. Hielscher, "Quasi-Newton methods in optical tomographic image reconstruction," *Inverse Probl.*, Vol. 19, No. 2, 2003.